5870 *Biochemistry* **2010,** *49,* 5870–5879
DOI: 10.1021/bi100432e

BIOCHEMISTRY
including biophysical chemistry & molecular biology
*Article*

# Analysis of the Crystal Structure of the ExsC·ExsE Complex Reveals Distinctive Binding Interactions of the *Pseudomonas aeruginosa* Type III Secretion Chaperone ExsC with ExsE and ExsD[†]

Nancy J. Vogelaar,[‡] Xing Jing,[‡] Howard H. Robinson,[§] and Florian David Schubot*,[‡]

[‡]*Department of Biological Sciences, Life Science I, Virginia Polytechnic Institute and State University, Washington Street, Blacksburg, Virginia 24060, and* [§]*Biology Department, Brookhaven National Laboratory, Upton, New York 11973-5000*

*Received August 17, 2009; Revised Manuscript Received June 8, 2010*

ABSTRACT: *Pseudomonas aeruginosa*, like many Gram-negative bacterial pathogens, requires its type III secretion system (T3SS) to facilitate acute infections. In *P. aeruginosa*, the expression of all T3SS-related genes is regulated by the transcriptional activator ExsA. A signaling cascade involving ExsA and three additional proteins, ExsC, ExsD, and ExsE, directly ties the upregulation of ExsA-mediated transcription to the activation of the type III secretion apparatus. In order to characterize the events underlying the signaling process, the crystal structure of the T3SS chaperone ExsC in complex with its cognate effector ExsE has been determined. The structure reveals critical contacts that mediate the interactions between these two proteins. Particularly striking is the presence of two Arg-X-Val-X-Arg motifs in ExsE that form identical interactions along opposite sides of an ExsC dimer. The structure also provides insights into the interactions of ExsC with the antiactivator protein ExsD. It was shown that the amino-terminal 46 residues of ExsD are sufficient for ExsC binding. On the basis of these findings, a new model for the ExsC·ExsD complex is proposed to explain its distinctive 2:2 stoichiometry and why ExsC displays a weaker affinity for ExsD than for ExsE.

The opportunistic pathogen *Pseudomonas aeruginosa* utilizes a diverse arsenal of virulence mechanisms to infect a broad range of hosts, including plants and mammals. In humans, predisposed individuals such as transplant and cancer patients are particularly susceptible to both chronic and acute *P. aeruginosa* infections (*1*−*5*). The bacterium is perhaps best known for causing the chronic lung infections in cystic fibrosis patients, which are the leading cause of mortality among this patient group (*6*). The formation of antibiotic-resistant biofilm colonies in the infected tissues is a hallmark of chronic infections. Acute *P. aeruginosa* infections, on the other hand, are characterized not by biofilm formation but are primarily supported by the bacterium's type III secretion system (T3SS)[1] (*7*−*10*). Recent evidence suggests that the T3SS also mediates the establishment of chronic infections, but once the biofilm colonies are formed, the T3SS becomes inactive (*11*−*13*). In *P. aeruginosa*, the T3SS translocates a combination of four possible enzymes, ExoS, ExoT, ExoU, and ExoY, into the host cells, where they act collectively to delay the host immune response at the site of infection (*14*−*18*).

Because production and maintenance of the T3SS are energy-intensive processes, bacteria exercise tight regulatory control over T3SS synthesis. A complex network of signaling pathways ensures that T3SS expression is stimulated at the onset of an infection. In *P. aeruginosa*, ExsA, an AraC/XylS-type transcriptional activator, controls the expression of all T3SS genes that encode the translocation apparatus, the secreted effectors, their chaperones, and several T3SS regulatory proteins, including ExsA itself (*19*−*22*). The most direct link between host-cell contact and upregulation of T3SS gene expression in *P. aeruginosa* is a four-protein signaling cascade involving the small secreted protein ExsE, its cognate chaperone ExsC, the antiactivator protein ExsD, and, at the bottom of the cascade, the transcription factor ExsA (*23*−*26*).

ExsE, an 8.7 kDa highly charged protein, alone has no well-defined tertiary structure as indicated by NMR and circular dichroism studies (*23*). Although secreted by the T3SS into target cells, ExsE has no known function beyond its role in the ExsA-ExsD-ExsC-ExsE signaling cascade.

ExsC is a 16.2 kDa protein that is a member of the type IA family of T3SS chaperones (reviewed in refs *24* and *25*). These chaperones are usually homodimeric and interact specifically with a single effector. InvB of *Salmonella typhimurium* and Spa15 of *Shigella flexneri* are members of class IB and, unlike class IA T3SS chaperones, associate with multiple effectors (*24*). Structures have been reported for a number of these T3SS chaperones (*26*−*31*), including five chaperone−effector complex structures (*32*−*36*). While type I chaperones have little sequence homology, they share a common fold that is characterized by a α-*β*-*β*-α-*β*-*β*-α topology. ExsC is unique among T3SS chaperones because, as part of the signaling process, ExsC interacts not only with ExsE but also with the nonsecreted antiactivator protein ExsD.

ExsD is a 31.4 kDa protein that forms a 1:1 complex with ExsA and is thought to act by preventing ExsA from interacting with its

[†]Funding for this work was provided by the start-up funds to Florian Schubot from the Virginia Polytechnic Institute and State University. Funding for data collected at beamline-29 NSLS is provided by DOE/DER and NIH/NCRR.

*Corresponding author. Phone: 540-231-2393. Fax: 540-231-4043. E-mail: fschubot@vt.edu.

[1]Abbreviations: DTT, dithiothreitol; EDTA, ethylenediaminetetraacetic acid; IPTG, isopropyl *β*-D-thiogalactopyranoside; MBP, maltose binding protein; PDB, Protein Data Bank; rms, root mean square; SAD, single-wavelength anomalous dispersion; SDS−PAGE, sodium dodecyl sulfate−polyacrylamide gel electrophoresis; Se-Met, selenomethionine; TCEP, tris(2-carboxyethyl)phosphine; TEV, tobacco etch virus; T3SS, type III secretion system.

 Published on Web 06/10/2010 

cognate promoters (*37*). The structure of ExsD was recently determined by this laboratory and found to resemble the DNA-binding transcriptional regulator KorB (*38*). At this time it not clear whether ExsD indeed binds to DNA as well as to ExsA or if the observed structural features are only a testament of the evolutionary origin of ExsD.

Prior to host-cell contact, the T3SS is inactive and ExsE and ExsC form a stable complex, while ExsA is kept inactive through its interactions with ExsD. Upon host-cell contact, ExsE is translocated through the T3SS causing the released ExsC molecules to sequester ExsD, thus permitting ExsA to initiate transcription from associated promoter sites (*39*−*42*). The apparent binding constants for the ExsE·ExsC and ExsD·ExsC complexes have been measured to be 1 and 18 nM, respectively, supporting the hypothesis that the signaling process is controlled by the relative binding affinities of the involved complexes. The ExsE·ExsC complex has been determined to have the 2:1 stoichiometry, typical for this type of complex. The unusual 2:2 stoichiometry of the ExsD·ExsC complex, on the other hand, suggests novel types of interactions (*23*, *43*). Binding of ExsE and ExsD to ExsC is mutually exclusive, but it is unknown whether they share the same binding site, whether they have overlapping binding sites, or if conformational changes in ExsC upon complex formation with one binding partner causes disruption of the binding site for the other binding partner.

The objective of the present study was to obtain structural insights into the ExsE·ExsC interactions that would allow us to identify distinctive features of the binding interface. These features revealed intriguing similarities between ExsE and the amino-terminal region of ExsD, which led us to propose a new model for the ExsD·ExsC complex that explains not only its unusual stoichiometry but also the weaker affinity of the ExsD·ExsC complex compared to the strength of the ExsE·ExsC interaction.

## EXPERIMENTAL PROCEDURES

*Cloning, Expression, and Purification of All ExsE·ExsC Complexes and the ExsD(1*−*46)·ExsC Complex*. *exsC*, *exsD*, and *exsE* were cloned from genomic *P. aeruginosa* DNA (ATCC 17933D) via PCR. ExsC and ExsE were co-overexpressed in *Escherichia coli* from a vector constructed by Gateway recombinational cloning (Invitrogen, Carlsbad, CA). Toward this end, a tobacco etch virus (TEV) protease-recognition site and the appropriate *att* recombination sites (*attB1* and *attB3*) were added to the *exsE* gene during PCR, and the resultant amplicon was recombined into *pDONR208* (Invitrogen) to produce *pDONR208-exsE*. PCR was also used to add a ribosome binding site and *attB3* and *attB2* sites to the *exsC* gene, which permitted cloning of this construct into *pDONR209* (Invitrogen) to yield the plasmid *pDONR209-exsC*. Precisely the same procedure as for *exsE* was followed for the cloning of the *exsD* gene and yielded the plasmid *pDONR208-exsD*. These three original plasmids for *exsC*, *exsE*, and *exsD* were subsequently used as templates to generate the variants described in this study. Point mutations were introduced via site-directed mutagenesis, while truncations were obtained by the use of appropriate primers in regular PCR reactions. The nucleotide sequences of all cloned constructs were verified through sequencing. The cloning constructs and primer sequences are tabulated in Supporting Information Table S1.

By recombining the *pDONR208-exsE* clones with the *pDONR-209-exsC* clones into the destination vector *pDEST-HisMBP* (*44*), a series of bicistronic expression vectors was created. These vectors were designed to produce ExsE and its variants as fusion proteins with the carboxy terminus of an amino-terminally His-tagged *E. coli* maltose-binding protein (MBP), removable by tobacco etch virus (TEV) protease. Similarly, *pDONR208-exsD(1*−*46)* was recombined with *pDONR209-exsC* into *pDEST-HisMBP* to yield *pDEST-HisMBP-exsD(1*−*46)-exsC*.

All protein complexes were produced by coexpressing ExsC with its intended binding partner in *E. coli* following the general methodology for recombinant protein production described by Tropea et al. (*45*). Briefly, *E. coli* BL-21(DE3) CodonPlus RIL cells (Stratagene) containing the bicistronic expression vector were grown to midlog phase at 37 °C in Luria broth containing 100 μg/mL ampicillin, 30 μg/mL chloramphenicol, and 0.2% glucose. Overproduction of each protein complex was initiated by the addition of isopropyl β-D-thiogalactopyranoside (IPTG) to 1 mM; cells were incubated for 5 h at 18 °C and then harvested by centrifugation (4 °C, 5000*g*, 15 min). Cells were stored at −80 °C if not used immediately. All of the following purification procedures were carried out at 4 °C. Cells were lysed in buffer A (25 mM Tris-HCl, 150 mM NaCl, 25 mM imidazole, 1 mM DTT, pH 7.4) with 5 μL/mL EDTA-free protease inhibitor cocktail (Sigma P8849). The cleared lysate was applied to a 30 mL Ni-NTA Superflow column (Qiagen) equilibrated with buffer A and eluted with a linear gradient to 250 mM imidazole. Peak elution fractions were combined, and His-TEV(S219 V)-$Arg_5$ protease (1 mg/100 mg of total protein) was added to effect the cleavage from His-MBP. The overnight TEV protease digestion was concomitantly dialyzed to reduce the imidazole concentration to 25 mM. The protein solution was then applied to a 40 mL Ni-NTA Superflow column (Qiagen). Flow-through fractions containing the protein complex were pooled, the salt concentration was lowered to 50 mM by dilution with 25 mM Tris-HCl and 1 mM DTT, pH 7.4, and the complex was further purified by anion-exchange chromatography using a 5 mL HiTrap-Q-HP column (GE Healthcare). The column was eluted with a linear salt gradient to 1 M NaCl. The complex was finally purified by size exclusion chromatography using a HiLoad 26/60 Superdex 200 column connected in series with a HiPrep 26/60 Sephacryl S-200 HR column (GE Lifesciences). The size exclusion and protein storage buffer (buffer B) contained 25 mM Tris-HCl, 150 mM NaCl, and 1 mM TCEP, pH 7.4.

The purification protocol for the ExsD(1−46)·ExsC complex was identical to the above procedure, except that the anion-exchange column step was omitted.

*Analytical Size Exclusion Chromatography*. For the comparative size exclusion analysis, samples of 10 μM solutions of ExsE·ExsC, MBP-ExsE·ExsC, MBP-ExsD(1−46) ·ExsC, and ExsD(1−46) ·ExsC were loaded individually onto a HiLoad 26/60 Superdex 200 column. Elution with buffer B was monitored via UV detection at 280 nm, and fractions were analyzed by SDS−PAGE.

*Preparation of Selenomethionine-Labeled Proteins*. Selenomethionine-substituted proteins were produced in the same nonauxotrophic strain of *E. coli* used for routine protein production. The incorporation of externally added selenomethionine into the recombinant ExsC was accomplished by suppressing methionine biosynthesis (*46*). The purification of selenomethionine-containing ExsE·ExsC complexes followed the same protocols as those of the unmodified complexes with the exception that the DTT concentration was increased to 2 mM.

*Limited Proteolysis of the ExsE·ExsC Complex*. A 1 mg/mL stock solution of thermolysin (Roche Molecular Biochemicals, Indianapolis, IN) in thermolysin buffer (10 mM Tris-HCl, 0.2 M NaCl, and 2 mM $CaCl_2$, pH 8.0) was used for the limited proteolysis experiments. The ExsE·ExsC stock solution consisted of

Table 1: Data Collection, Phasing, and Structure Refinement Statistics

| | Δ15ExsE·ExsC133-D132A | Se-Met 15ExsE·ExsC133-D132A-L45M-L54M |
|---|---|---|
| **Data Collection Statistics** | | |
| molecules/asymmetric unit | 6 | 6 |
| atoms/asymmetric unit | 15016 | |
| wavelength (Å) | 1.0809 | 0.9789 |
| space group | $P2_12_12_1$ | $P2_12_12_1$ |
| unit cell parameters (Å) | $a$ = 96.3 | $a$ = 96.3 |
| | $b$ = 125.0 | $b$ = 116.7 |
| | $c$ = 228.1 | $c$ = 230.7 |
| resolution (Å) (last shell) | 30−2.8 (2.9−2.8) | 30−3.0 (3.11−3.00) |
| total reflections | 687995 | 644950 |
| unique reflections | 66241 (5652) | 51116 (3925) |
| completeness (%)[a] | 97.0 (83.6) | 95.9 (74.6) |
| redundancy | 10.4 (5.3) | 12.6 (7.5) |
| average $I/\sigma I$ | 24.7 (1.6) | 19.5 (1.9) |
| $R_{merge}$ (%)[b] | 8.0 (49.8) | 12.6 (59.3) |
| data cutoff | $F > 0$ | $F > 0$ |
| **Phasing Statistics** | | |
| no. of selenium sites | N/A | 38 |
| overall FOM (RESOLVE)[c] | | 0.62 |
| $R$ (%)[d] (Se atom substructure) | | 32.9 |
| **Refinement Statistics** | | |
| resolution range (Å) | 30−2.80 | N/A |
| last shell | 2.87−2.80 | |
| $R_{free}$ (%)[e] | 25.7 (36.8) | |
| $R_{work}/R_{free}$ | 0.844 (0.864) | |
| bond lengths, rms deviation (Å) | 0.002 | |
| bond angles, rms deviation (deg) | 0.48 | |
| no. of water molecules | 89 | |
| residue average temperature factor (Å$^2$) | 87.4 | |
| water molecule temperature factor (Å$^2$) | 54.0 | |
| Ramachandran analysis | | |
| residues in preferred regions | 1517 | |
| residues in additional allowed regions | 158 | |
| residues in generously allowed regions | 0 | |
| residues in disallowed regions | 0 | |

[a]The values in parentheses relate to the highest resolution shell. [b]$R_{merge} = [\sum|I - \langle I\rangle|]/\sum I$, where $I$ is the observed intensity and $\langle I\rangle$ is the average intensity obtained from multiple observations of symmetry-related reflections after the rejection of significant outliers. [c]Figure of merit as defined by Blundell and Johnson (*58*), averaged over all reflections. For each reflection, FOM = $\langle\cos\Delta\varphi\rangle$, where $\Delta\varphi$ is the error in phase angle. [d]$R = [\sum||F_o| - |F_c||]/\sum|F_o|$, where $F_o$ and $F_c$ are the observed and calculated structure factors, respectively. [e]$R_{free}$ defined by Brunger (*59*).

the protein at 1 mg/mL in buffer A. The five individual reactions were composed of 25 μL of ExsE·ExsC stock solution, 25 μL of 2× thermolysin buffer, and 0.5 μL of serial 1:4 dilutions of the thermolysin stock solution. The reactions were allowed to proceed for 1 h at 37 °C before the protease was inactivated by the addition of 0.5 μL of 0.5 M EDTA. The reaction products were initially visualized by SDS gel electrophoresis. The precise molecular weights of select fragments were determined using LC-electrospray ionization-MS. Five micrograms of protein in 5 μL of buffer B was loaded onto the $C_4$ reversed-phase column (Grace Vydac, 214MS5205) at 200 μL/min and eluted with a linear gradient from 0% to 80% acetonitrile in 0.1% formic acid. The mass spectrometer was an ABI/MDS-Sciex 3200 QTrap with a Sciex TurboSpray ion source operating at a voltage of 5500 V. A 4000 amu/s scan speed was used. The peptide molecular mass was determined by deconvolution of the mass spectrum using BioAnalyst version 1.1 (ABI) and the proteolytic product identified using the FindPep program (*47*).

*Protein Crystallization*. Diffraction quality crystals of the Δ15ExsE·ExsC133-D132A and the selenomethionine-labeled Δ15ExsE·ExsC133-D132A-L45M-L54M complexes were both obtained using the hanging drop method with initial droplets created by mixing 1.5 μL of protein (20.0 mg/mL) with 0.5 μL of a crystallization solution composed of 1.0 M sodium potassium tartrate, 0.2 M lithium sulfate, and 0.1 M CHES, pH 9.0. Crystals appeared after 3 days at 10 °C and could be harvested after 1−2 weeks.

*X-ray Data Collection, Structure Solution, and Refinement*. Crystals were loop-mounted without cryosoaking and flash-cooled in liquid nitrogen. Data sets were collected at beamline X-29A of the National Synchrotron Light Source using an ADSC Q315 CCD detector. Data processing was done using the HKL2000 program suite (*48*). Details of data collection and processing for all data sets are provided in Table 1. The Se-Met-Δ15ExsE·ExsC133-D132A-L45M-L54M structure was determined using the single-wavelength anomalous dispersion (SAD) method, and the location of heavy atom positions, initial phase calculations, phase improvement through density modification, and initial maps were calculated using the PHENIX program suite (*49*). Nearly all of the ExsC133-D132A-L45M-L54 M dimer

backbone could be traced for one molecule, and six copies of the resulting model could be placed by PHENIX into the asymmetric unit using molecular replacement.

All six ExsC dimers were then used to solve the 2.8 Å Δ15ExsE·ExsC133-D132 structure using molecular replacement. The final model was obtained after several cycles of manual adjustment of the model using COOT (*50*) followed by refinement using PHENIX. The Δ15ExsE chains were built as the electron density in weighted difference-Fourier maps improved over the course of refinement. Model quality was assessed with PROCHECK (*51*), and the atomic coordinates and structure factors for the Δ15ExsE·ExsC133-D132A structure have been deposited in the Protein Data Bank (PDB) (*52*) with accession code 3kxy.

## RESULTS AND DISCUSSION

*Determination of the Crystal Structure of the ExsE·ExsC Complex*. Initially, the ExsE·ExsC complex crystallized with remarkable ease. Several conditions yielded large needle-shaped crystals. However, these crystals proved extremely fragile, and the collection of X-ray diffraction data beyond a resolution of 4 Å was unsuccessful. In addition, the obtained diffraction patterns were highly anisotropic, suggesting poor packing contacts in at least one direction. We sought to define the domain boundaries of both proteins by subjecting the complex to limited proteolysis with thermolysin and analyzing select degradation products via electrospray mass spectrometry. The results of our analysis led us to truncate the first 15 amino acids of ExsE, which presumably correspond to its secretion signal, and to remove carboxy-terminal residues 140−144 from ExsC. We further improved the quality of our crystals by creating and screening a number of surface entropy reduction mutants of ExsC. To this end we identified stretches of sequence containing clusters of residues with notoriously flexible side chains such as lysine, arginine, and glutamate and mutated these to alanines. Ultimately, the successful ExsC mutant combined the surface-entropy lowering mutation D132A with a further truncation that removed three high-entropy residues Asp-134, Arg-135, and Glu-136. At 2.8 Å resolution, the best diffraction data were obtained for crystals of this complex, Δ15ExsE·ExsC133-D132A. These data were ultimately used for model building and refinement.

Structure solution was initially attempted through molecular replacement using a variety of search models for both the ExsC monomer and dimer. No solution could be obtained, probably because of the large size of the asymmetric unit, which contains six independent ExsE·ExsC complexes. Therefore, it became necessary to prepare selenomethionine-derivatized protein crystals for SAD-based structure solution.

Not including the start codon, the sequence of ExsC133-D132A contains only a single methionine residue, and ExsE contains no methionine. In view of the high noncrystallographic symmetry of the crystals, we had, nevertheless, hoped that a selenomethionine derivative of this complex would be sufficient for structure solution. X-ray diffraction data collected with crystals containing the selenomethionine-derivatized Δ15ExsE·ExsC133-D132A complex failed to yield interpretable electron density maps, however. We therefore engineered two additional methionine residues into ExsC to produce selenomethionine-labeled Δ15ExsE·ExsC133-D132A-L45M-L54M. The modified sample readily crystallized, and 3.0 Å selenium peak data yielded interpretable electron density maps when analyzed with the PHENIX program suite (*49*). For one of the six Δ15ExsE·ExsC133-D132A-L45M-L54M molecules, nearly all of the ExsC dimer backbone could be traced and many side chains identified and positioned. Phased molecular replacement was used to place the other five ExsC dimers into the asymmetric unit. Because higher resolution diffraction data had been collected for crystals of an unlabeled Δ15ExsE·ExsC133-D132A complex, model building and refinement were carried out with this data set. The final model is composed of 1897 of the 1992 residues. Model refinement statistics are given in Table 1. All residues reside either in the most favorable or in the allowed regions of the Ramachandran plot, and the overall geometry was better than average when compared to structures solved at the same resolution. It is of note that the ExsE·ExsC structure has an overall *B* factor that is at the high end of the expected range for structures at this resolution. The *B* factors for the individual protein chains ranged from 54 to 130 Å$^2$, with the chains with highest *B* factors having few crystal contacts.

To confirm that the truncations to ExsC and ExsE had not eliminated residues that are important to the ExsE·ExsC interface, we determined the crystal structure of full-length ExsE·ExsC at 4 Å resolution using molecular replacement and observed no additional main-chain density at either the amino terminus of ExsE or the carboxyl terminus of ExsC (unpublished results).

*Structural Description of the ExsE·ExsC Complex*. The structure of the Δ15ExsE·ExsC133-D132A complex is depicted in Figure 1a. Similar to other T3SS chaperone−effector complexes, ExsC forms a compact homodimer, and ExsE is wrapped around one face of this dimer in an extended conformation with $\beta$2 and $\beta$3 strands of ExsE interacting with the $\beta$1 strands of the ExsC dimer. The entire Δ15ExsE molecule participates in the binding of ExsC. The binding of ExsE to the ExsC homodimer causes the two ExsC molecules in the complex to be nonequivalent. In the following discussion, when the monomers are discussed individually, unmarked references to ExsC will denote the ExsC molecule that interacts predominantly with the amino terminus of ExsE, and a prime (ExsC′) will denote the ExsC molecule that interacts with the carboxy terminus of ExsE. Each ExsC monomer is folded into a five-stranded antiparallel twisted $\beta$ sheet flanked by three α helices. The observed α1-$\beta$1-$\beta$2-$\beta$3-α2-$\beta$4-$\beta$5-α3 topology is typical for this family of T3SS chaperones (Figure 1). The formation of the symmetric ExsC dimer interface is mediated by interactions between the α-2 helix of each monomer with the α-2 helix and $\beta$-5 strand of the other ExsC molecule. The structures of the ExsC and ExsC′ molecules are quite similar to one another. When ExsC monomers are superposed pairwise within each complex using Cα positions 3−130, the average rms deviation in the ExsC−ExsC′ Cα position for all six complexes is 1.2 ± 0.2 Å. The regions of ExsC and ExsC′ that differ the most are those that interface differently with ExsE, particularly residues 71−80 which have an rms deviation of 2.2 ± 1.2 Å in their Cα positions.

Although the presence of six independent complexes in the asymmetric unit complicated the model-building process, their comparison provides valuable insight into the dynamics of the ExsE·ExsC interaction. ExsE is anchored by strand−strand interactions with ExsC at both its amino terminus and carboxy terminus. These contacts are characteristic of this type of complex (*33*), and residues 17−33 and 70−81 are well-defined in all six ExsE·ExsC complexes. Differences between the complexes emerge as we follow the ExsE chain across the face of the chaperone dimer. In three of the six complexes, much of the region between residues 34 and 65 produced such poor electron

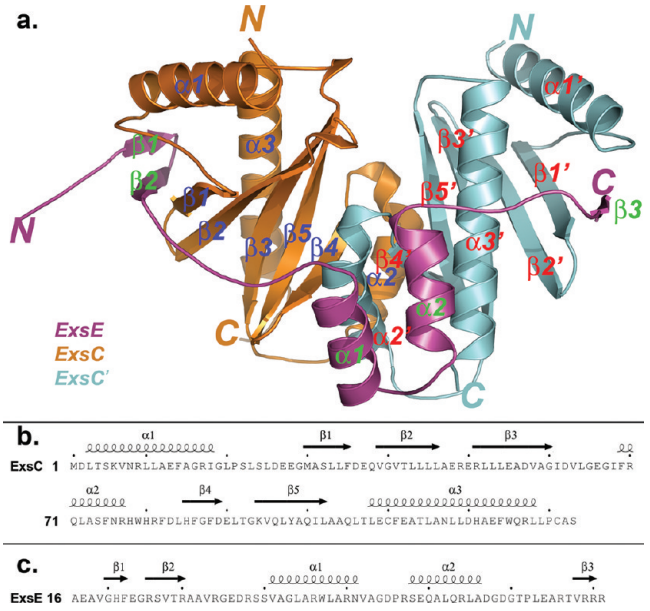


FIGURE 1: The ExsE·ExsC structure. (a) PYMOL-generated (*60*) cartoon representation of the ExsC(1−133)D132A·Δ15ExsE complex structure. The two molecules of the ExsC dimer are colored orange and cyan, respectively, while the ExsE fragment was given a purple color. All secondary structure elements are labeled, and elements of the ExsC molecule that associates with the carboxy terminus of ExsE have been marked with a prime (′). (b, c) Alignment of the secondary structure elements identified from the crystal structure with the primary structures of ExsC and ExsE, respectively. These were generated with ESPript (*61*).

density that reliable modeling proved impossible. In the other three complexes, all or most of that region could be traced and was seen to fold into two α-helices. The positions of these helices relative to the ExsC dimer were variable, however. A superposition of the six independent ExsE·ExsC complexes can be seen in Figure 2a. The underlying reason for the observed differences in the quality of the electron density for the six ExsE molecules may be found in the crystal-packing arrangement. The well-ordered ExsE molecules mediate contacts with neighboring complexes, while the partially disordered ExsE molecules are surrounded by solvent alone and are, therefore, less conformationally constrained.

The ExsE·ExsC structure was compared to the currently known structures of other T3SS chaperones and chaperone−effector complexes. Structures have been reported for the chaperones SigE (*26*) from *Salmonella enterica*, CesT (*27*) from *E. coli*, Spa15 (*28*) from *S. flexneri*, AvrPphF ORF1 from *Pseudomonas syringae* (*29*), SycE from *Y. pestis* (*30*), and SycT (*31*) from *Y. enterocolitica*. Several chaperone-effector complex structures have also been determined: SicP·SptP from *S. enterica* (*32*), InvB·SipA from *Salmonella* (*33*), SycN·YscB·YopN (*34*), and SycE·YopE from *Yersinia pseudotuberculosis* (*35*). All four complexes display a 2:1 chaperone-to-effector stoichiometry, where the chaperone-binding domain of the effector molecule has little or no tertiary structure and is wrapped around the chaperone dimer in an extended conformation. The SycH·YscM2 structure from *Yersinia pestis* constitutes the only example for a complex with 2:2 stoichiometry. However, this unusual stoichiometry was probably an artifact caused by YscM2 truncation (*36*).

When compared to the other T3SS chaperone structures, the ExsC dimer was confirmed to be a T3SS class IA chaperone by the relative orientation of its subunits (*24*, *28*). The ExsC dimer most closely resembles SicP in the SicP·SptP complex (*32*). The rms deviation for equivalent Cα atoms is 2.2 Å for the superposed chaperone monomers and 2.6 Å for the superposed dimers. The paths of T3SS effectors across the face of their chaperone dimers are quite variable. The path of ExsE across the ExsC dimer is similar to that taken by YopN across the face of its heterodimeric chaperone SycN·YscB (*34*). Both T3SS effectors are anchored on the amino- and carboxy-terminal regions of their chaperone-binding domain (CBD) to their chaperones by strand−strand interactions (*33*). Between these anchors, the effectors assume an extended conformation with helical regions. Like some of the ExsE·ExsC complexes in the current structure, YopN is locally disordered where it crosses the interface between the two chaperone molecules, and 11 of its residues could not be modeled. Similar localized disorder in this region has also been observed in the SipA·InvB complex.

*Examination of the ExsE·ExsC Interface*. The interface for the ExsE·ExsC interaction is variable due to the observed disorder in the structure and ranges from 1725 Å$^2$ for the complex that includes only the most structurally conserved parts of ExsE (residues 17−39 and 68−81) to 2465 Å$^2$ for the complex containing the fully traced ExsE molecule. Although contacts from the dynamic region of ExsE (residues 40−67) may indeed contribute to the stability of the ExsE·ExsC complex, we reason that the most important interactions for complex formation and stability will be those preserved in all six independent complexes. Consequently, our analysis focused on these conserved features. Toward that end, we generated lists of the ExsE·ExsC contacts for all six complexes (Supporting Information File S2). From these tables we extracted a surprisingly small number of conserved interactions which are summarized in Figure 2. If the two ExsC monomers of the ExsE·ExsC complex are superimposed, the $\beta$ strands consisting of ExsE residues 25−31 and 75−81 overlay with a Cα rms deviation of 1.4 Å. The superposition of these regions can be seen in Figure 2e. The protein−protein interfaces associated with these two regions of ExsE will be referred to as site 1 and site 2, respectively.

The strand−strand interactions between ExsE and ExsC are mediated by three main-chain to main-chain hydrogen bonds in each site, and they are likely to be critical to the stability of the complex. Side-chain interactions, however, confer binding specificity and mediate contacts between ExsE and the α3 helices of the ExsC dimer. Here, two Arg-X-Val-X-Arg motifs in ExsE that form nearly identical contacts along opposite sides of the ExsC dimer appear to play a pivotal role. In site 1, ExsE Arg-26 forms salt bridges with the side chains of Asp-120 and Glu-123 of ExsC, while Arg-30 hydrogen bonds with the carbonyl group of Ser-24 of ExsC. Remarkably, this interaction pattern is faithfully repeated in site 2 as indicated in Figure 2b. Main-chain atoms of ExsE Ser-27 and Thr-77 also form identical contacts with the side chains of the two ExsC Asp-36 residues, but, because these interactions do not involve the side chains of these ExsE residues, their chemical similarity may be coincidental. Additional contacts unique to each site further enhance the Arg-X-Val-X-Arg binding motif (Figure 2b,c).

One interaction between ExsE and ExsC that is conserved in other T3SS effector−chaperone complexes as well as in all six ExsE·ExsC complexes is the van der Waals interaction between a hydrophobic patch on the chaperone surface and a hydrophobic side chain of the effector. In the case of the ExsE·ExsC complex, the ExsC hydrophobic patch is composed of residues Phe-14, Phe-23, and Phe-35, and the hydrophobic ExsE residues are Phe-23 and Leu-73 for sites 1 and 2, respectively.

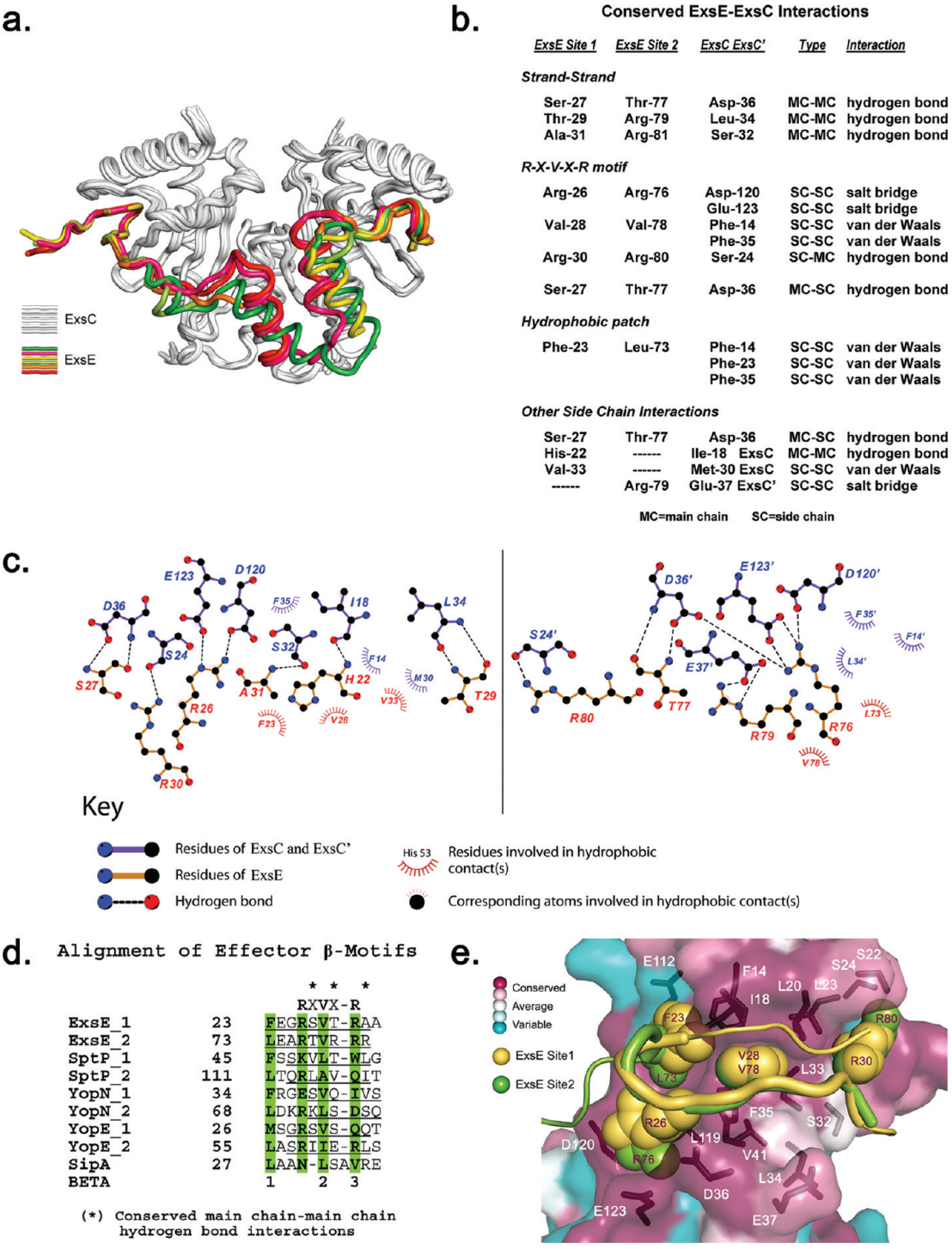


FIGURE 2: The ExsE·ExsC molecular interface. (a) Superposition of all six independent molecules of the ExsC(1−133)D132A·Δ15ExsE complex structure, showing the variability in the central region of the ExsE molecule. ExsC and ExsC′ subunits have been depicted in white and the ExsE molecules in color. This cartoon drawing was prepared using PYMOL (*60*). (b) Conserved interactions between ExsE and ExsC. Site 1 ExsE residues interact with ExsC, and site 2 ExsE residues interact with ExsC′. (c) LIGPLOT-generated (*62*) schematic of the interactions of ExsE with ExsC and ExsC′, respectively. Shown are only those main-chain and side-chain interactions that occur in all six complexes and are thus likely pivotal for the stability of the complex. A complete list of all contacts in the six complexes is provided in Supporting Information File S2. The maximum distance cutoffs were 3.9 Å for van der Waals contacts and 2.5 Å for hydrogen-acceptor bonds. Note that, at a resolution of 2.8 Å for the X-ray diffraction data, no hydrogen atoms can be observed in the electron density map. Instead, distances are measured between non-hydrogen donor−acceptor atoms under the assumption that the hydrogen atom is present and bound to the donor atom at a bond length of 1 Å (i.e., a 2.5 Å hydrogen bond is reflected in a 3.5 Å donor−acceptor distance). These specific distance cutoffs were chosen because they represent the reasonable default values used by LIGPLOT. (d) Structure-based sequence alignment of all effector β-motif regions for currently known effector−chaperone complexes. Residues of the effector half-sites that superpose when the two chaperone molecules of the complex are superposed are underlined. The Arg-X-Val-X-Arg motif is shown along with β-motif residues identified by Lilic et al. (*33*). (e) The effector−chaperone binding region of the ExsE·ExsC structure. The ExsC surface is colored according to a normalized residue conservation score as determined by Consurf (*53*) using its maximum likelihood algorithm and based on a DaliLite-generated (*54*) structural alignment of 13 T3SS chaperones including ExsC (Supporting Information File S3). The path of the effector is depicted as a cartooned tube with the β-motif region indicated as a thickened tube. Both effector−chaperone binding sites are shown simultaneously by displaying the relevant ExsE regions of the superposed ExsC monomers. Important effector side chains are shown as space-filling spheres.

When examining the structure of the SipA·InvB complex, Lilic et al. (*33*) identified a conserved $\beta$-motif in the chaperone-binding domains of T3SS effectors that partially overlaps ExsE·ExsC's Arg-X-Val-X-Arg motif. This $\beta$-motif is generally eight residues long and anchors the effector to a hydrophobic crevice in the chaperone through three hydrophobic residues, which herein will be designated $\beta$1, $\beta$2, and $\beta$3. A structure-based alignment of this $\beta$-motif region from all known effector−T3SS chaperone structures is shown in Figure 2d. This figure also shows the relative positioning of ExsE·ExsC's Arg-X-Val-X-Arg motif. In ExsE, the $\beta$2 and $\beta$3 positions are occupied by the valine and the second arginine of the Arg-X-Val-X-Arg motif, while ExsE residues Phe-23 and Leu-73 constitute the $\beta$1 residues. The positions occupied by ExsE Arg-26 and Arg-76, the first arginines in the Arg-X-Val-X-Arg motifs, are not discussed by Lilic et al. However, an examination of the corresponding residues in the other effectors shows a striking propensity for charged, especially positively charged, amino acids at this site. In most cases these charged residues form salt bridges with negatively charged residues in their respective chaperones. In ExsC the corresponding residues are Asp-36 and Glu-123. SipA's Asn-30 and YopN's site1 Glu-37 are the exceptions because they form hydrogen bonds with residues in their chaperones.

T3SS chaperones display overall low levels of sequence conservation. Yet, the residues that interact with the $\beta$-motif are generally well conserved as illustrated in Figure 2e. Residue conservation was assessed by the ConSurf web server (*53*) using an input of a DALI-generated (*54*) structure-based alignment of 13 available chaperone structures (Supporting Information File S3). The relative conservation of residues that line the effector binding cleft is apparent, along with residues corresponding to ExsC Asp-36 and Glu-123. Lilic et al. (*33*) noted the variation in the nature of the $\beta$3 residue, and a similar variability is observed in that region of the chaperone corresponding to ExsC residue Ser-24.

*Residues 1−46 of ExsD Are Sufficient for Stable ExsC·ExsD Complex Formation*. ExsC stands out among T3SS chaperones because it associates not only with its cognate effector ExsE but also with the antiactivator protein ExsD. The ExsD·ExsC complex displays some distinctive features, including an unusual 2:2 stoichiometry and the fact that, despite its interaction with a T3SS chaperone, ExsD is not secreted. Some similarities to conventional chaperone−effector complexes have emerged, however. ExsD competes with ExsE for binding to ExsC, albeit with 18-fold lower affinity (*23*) and a mutational analysis aimed at mapping the ExsD·ExsC interface identified ExsD residue pair Arg-18/Arg-19 as important for ExsC binding, suggesting that, just as in more conventional effector molecules, the amino terminus of ExsD is involved in chaperone binding (*43*). We recently solved the crystal structure of ExsD and found it had a well-defined and largely α-helical structure between residues 37 and 276, including a 40 Å coiled coil. This structure, in conjunction with a limited proteolysis experiment, revealed that the 36 amino-terminal residues of ExsD are not structured (*38*). This observation is interesting because this type of structural disorder is common among T3SS chaperone-binding domains in the absence of their cognate binding partner (*55*). An examination of the sequence of the unstructured region revealed remarkable parallels between this section of ExsD and ExsE: Δ15ExsE contains 12 arginine residues, comprising 19% of the entire 66 residue construct. As discussed in the previous section, at least five of these arginines, Arg-26, Arg-30, Arg-76, Arg-80, and Arg-81, are important for ExsC binding. Remarkably, arginine residues also account for 6 of the 40 amino-terminal ExsD residues. An alignment of the ExsD amino terminus with ExsE revealed clear sequence similarities between residues 23−45 of ExsE and residues 15−37 of ExsD. The stretch of ExsE that aligns with ExsD has been colored red in the ExsE·ExsC structure (Figure 3a). Also shown are the side chains of residues that are conserved between the two (Figure 3a). The pairwise alignment of the N-terminal region of ExsD with ExsE can be seen in Figure 3b. The two aligned sequences show a 22.5% sequence identity without gaps. Contained within this stretch is one of ExsE's two Arg-X-Val-X-Arg motifs and the universally conserved $\beta$-motif described in the previous section. The Arg-X-Val-X-Arg motif is not fully conserved in ExsD, but Arg-18 and Val-20 of ExsD do align with Arg-26 and Val-28, respectively, of ExsE. As stated above, residues Arg-17/Arg-18 of ExsD have previously been shown to be important for ExsC binding (*43*). Based on the alignment, ExsD actually gives a better agreement with the $\beta$-motif as described by Lilic et al. than ExsE because the three putative $\beta$-motif residues Phe-15, Val-20, and Leu-22 of ExsD are all hydrophobic.

In order to validate our hypothesis that the amino terminus of ExsD indeed constitutes a critical part of the chaperone-binding domain, we coexpressed and copurified the 46 amino-terminal residues of ExsD(1−46) with ExsC. We observed a stable complex that readily purified and eluted as a single peak from a size exclusion column. This peak was analyzed via SDS−PAGE, and two bands were observed at the expected molecular weights (Figure 3c, lane 3). Subsequently, we sought to confirm that the truncated ExsD(1−46)·ExsC complex had retained the unusual stoichiometry of the full-length complex using size exclusion chromatography. Initially, to establish that both complexes did not significantly differ in their shapes, we compared the elution profile of the ExsD(1−46)·ExsC complex (MW = ∼42 kDa for an assumed 2:2 stoichiometry) with that of the ExsE·ExsC complex (MW = ∼40 kDa for a 1:2 stoichiometry). Because the predicted molecular masses of both complexes are very similar, both eluted at very similar volumes at 243 and 244 mL, respectively (Figure 3d). Subsequently, we took advantage of the fact that ExsD(1−46) and ExsE are both initially expressed as $His_6$-MBP fusion proteins. We reasoned that if the $His_6$-MBP-ExsD-(1−46)·ExsC complex has a 2:2 stoichiometry, this complex should contain an additional MBP molecule compared to the $His_6$-MBP-ExsE·ExsC complex, which a possesses a well-established 2:1 chaperone:effector stoichiometry. Consequently, $His_6$-MBP-ExsD(1−46)·ExsC should elute substantially earlier from the size exclusion column than $His_6$-MBP-ExsE·ExsC. This was indeed observed with the $His_6$-MBP-ExsD(1−46)·ExsC eluting at 219 mL compared to the 230 mL observed for the MBP-ExsE·ExsC complex. Taken together, these experimental findings are consistent with our hypothesis that the amino terminus of ExsD constitutes a critical part of the chaperone-binding domain and that the ExsD(1−46)·ExsC complex retains the stoichiometry of the native ExsD·ExsC complex.

Above results may also explain the several features of the ExsD·ExsC complex. The ordered part of the ExsD crystal structure starts at residue 37, which, according to our sequence alignment, would correspond to residue 45 of ExsE, located in the mobile helical region of the latter molecule. If residues 15−37 of ExsD are indeed functionally equivalent to amino acids 23−45 of ExsE, the 36-residue unstructured region of ExsD would be too short to reach the second binding site along the other side of the

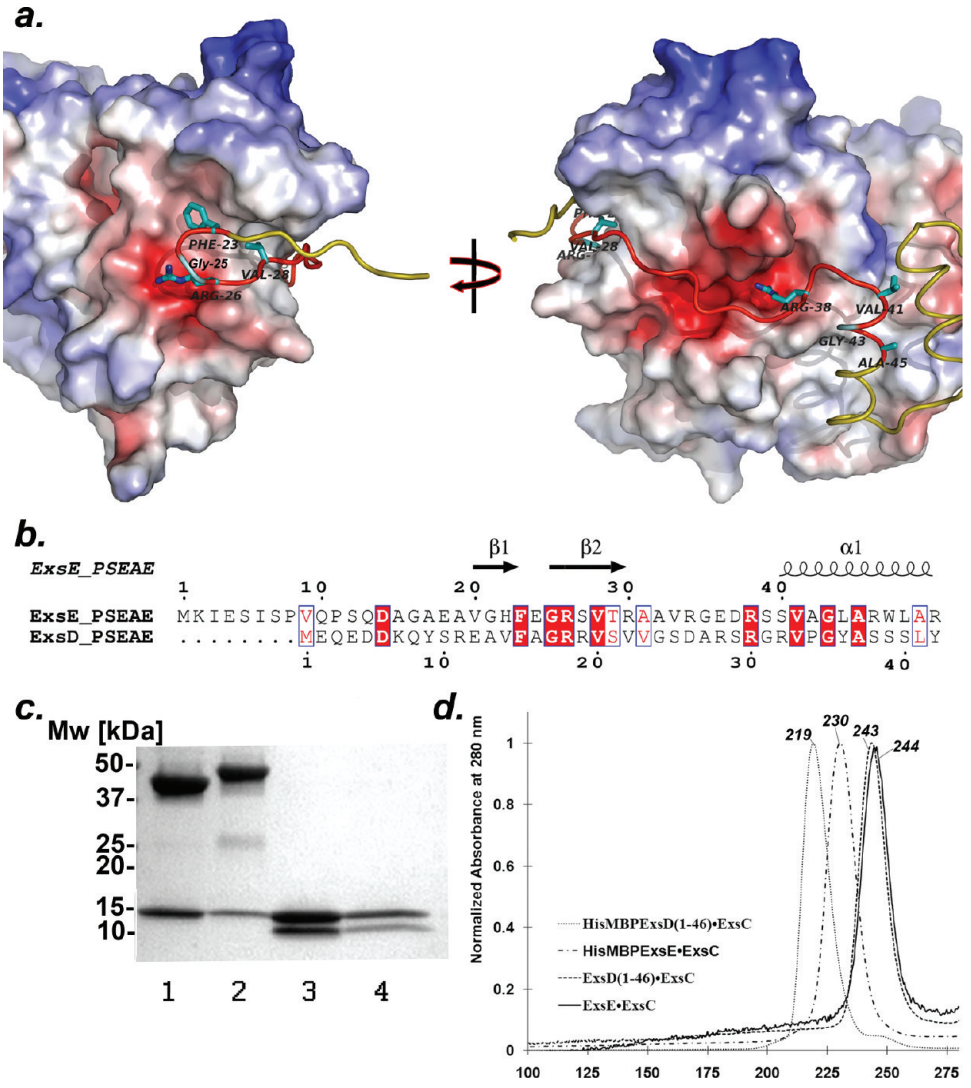


FIGURE 3: Comparison of ExsD and ExsE. (a) Two partial views of the ExsE·ExsC complex structure, focusing on the interactions between the amino terminus of ExsE and ExsC. The solvent-accessible surface area of ExsC is colored according to its electrostatic surface potential using a −8 to +8 kT/e range, while the backbone region of ExsE that aligns with ExsD has been colored red. The side chains of residues that are conserved between ExsE and ExsD are also shown. (b) A pairwise alignment between the amino terminus of ExsD and ExsE, including the corresponding secondary structure elements in ExsE reveals a number of conserved residues, suggesting similarities between the ExsE·ExsC and ExsD·ExsC complexes. (c) SDS−PAGE analysis of the size exclusion profiles in (d). Lanes: (1) $His_6$-MBP-ExsD(1−46)·ExsC; (2) $His_6$-MBP-ExsE·ExsC; (3) ExsD(1−46)·ExsC; (4) ExsE·ExsC. (d) Size exclusion profiles of ExsC complexed with $His_6$-MBP-ExsD(1−46), $His_6$-MBP-ExsE, ExsD(1−46), and ExsE. Similar elution profiles for ExsE·ExsC and ExsD(1−46)·ExsC are consistent with their similar molecular weights. The earlier elution of the $His_6$-MBP-ExsD(1−46)·ExsC complex compared to the 1:2 $His_6$-MBP-ExsE·ExsC complex is indicative of a 2:2 $His_6$-MBP-ExsD(1−46):ExsC stoichiometry.

ExsC dimer. While confounding at first, this observation may actually explain the unorthodox 2:2 stoichiometry of the ExsD·ExsC complex. As described previously, a single chaperone-binding domain usually wraps around the entire face of the chaperone dimer, forming characteristic strand−strand interactions with both ExsC monomers, thus explaining the 2:1 chaperone-to-binding partner stoichiometry (*25*, *32*−*35*, *56*). However, if ExsD does not possess the second half of the typical chaperone-binding domain, a second ExsD molecule could bind along the other face of the ExsC dimer forming a symmetric 2:2 complex. There is one example of a 2:2 chaperone−effector complex: *Y. pestis* chaperone SycH forms a stable 2:2 complex with the truncated regulatory protein YscM2 (*36*). Similar to other effector proteins, the 20-residue chaperone-binding domain of YscM2 forms strand−strand contacts with its chaperone and also binds to a shallow groove along one face of the SycH dimer. Because of its short length, YscM2 does not extend into the second strand interaction site, permitting a second YscM2 molecule to bind to the SycH dimer. This model is particularly appealing because it would not only explain the unusual stoichiometry of the ExsD·ExsC complex but the smaller predicted ExsD·ExsC binding interface might also account for the lower affinity of ExsD for ExsC compared to that of the ExsE·ExsC complex. Furthermore, the overlapping binding sites readily explain why the two complexes are mutually exclusive.

In conclusion, the ExsACDE signaling cascade constitutes an important regulatory switch that ensures timely expression of the T3SS and thus plays a critical role in facilitating *P. aeruginosa* infections. As part of our effort to elucidate the molecular basis of the signaling process, we have solved the crystal structure of a complex between the T3SS chaperone ExsC and its cognate binding partner ExsE. This structure provided a detailed map of the protein−protein interface and permitted the identification of two Arg-X-Val-X-Arg ExsC-binding motifs in ExsE, which

constitute an extension of the previously reported conserved $\beta$-motif for similar complexes. Furthermore, the structural analysis revealed similarities between critical residues in ExsE and the amino terminus of the antiactivator protein ExsD. On the basis of these similarities we proposed a new model for an ExsD·ExsC complex that was validated by a characterization of an ExsD(1−46)·ExsC complex.

## ACKNOWLEDGMENT

The authors thank Dr. Benjamin Orsburn for assistance with the mass spectrometry work.

## SUPPORTING INFORMATION AVAILABLE

One table containing all clones used in this study and the sequences of all primers that were used to generate these clones (S1); an excel file containing six spreadsheets, one for each ExsE·ExsC complex in the asymmetric unit (using the program CONTACT from CCP4 (*57*), all intermolecular contacts between ExsE and the two associated ExsC molecules were calculated using a distance cutoff of 3.9 Å; the data contained in this file were used to construct Figure 2c) (S2); structure-based sequence alignment generated by DaliLite that was used as input to ConSurf for residue variability analysis and display (structure and chains included 3kxyA (ExsC-chainA, this work), 1jyoA, 3epuA, 1xkpC, 1ttwA, 2bsjA, 1s28A, 1xkpB, 1n5bA, 1k3sA, 1ry9A, 2fm8A, and 1k3eB) (S3). This material is available free of charge via the Internet at http://pubs.acs.org.

## REFERENCES

1. Richards, M. J., Edwards, J. R., Culver, D. H., and Gaynes, R. P. (1999) Nosocomial infections in medical intensive care units in the United States. National Nosocomial Infections Surveillance System. *Crit. Care Med. 27*, 887–892.
2. Crouch Brewer, S., Wunderink, R. G., Jones, C. B., and Leeper, K. V., Jr. (1996) Ventilator-associated pneumonia due to *Pseudomonas aeruginosa*. *Chest 109*, 1019–1029.
3. Labrec, E. H., Schneider, H., Magnani, T. J., and Formal, S. B. (1964) Epithelial cell penetration as an essential step in the pathogenesis of bacillary dysentery. *J. Bacteriol. 88*, 1503–1518.
4. Garau, J., and Gomez, L. (2003) *Pseudomonas aeruginosa* pneumonia. *Curr. Opin. Infect. Dis. 16*, 135–143.
5. Cheng, K. H., Leung, S. L., Hoekman, H. W., Beekhuis, W. H., Mulder, P. G., Geerards, A. J., and Kijlstra, A. (1999) Incidence of contact-lens-associated microbial keratitis and its related morbidity. *Lancet 354*, 181–185.
6. Gomez, M. I., and Prince, A. (2007) Opportunistic infections in lung disease: *Pseudomonas* infections in cystic fibrosis. *Curr. Opin. Pharmacol. 7*, 244–251.
7. Hauser, A. R., Cobb, E., Bodi, M., Mariscal, D., Vallâes, J., Engel, J. N., and Rello, J. (2002) Type III protein secretion is associated with poor clinical outcomes in patients with ventilator-associated pneumonia caused by *Pseudomonas aeruginosa*. *Crit. Care Med. 30*, 521–528.
8. Holder, I. A., Neely, A. N., and Frank, D. W. (2001) Type III secretion/intoxication system important in virulence of *Pseudomonas aeruginosa* infections in burns. *Burns: J. Int. Soc. Burn Injuries 27*, 129–130.
9. Roy-Burman, A., Savel, R. H., Racine, S., Swanson, B. L., Revadigar, N. S., Fujimoto, J., Sawa, T., Frank, D. W., and Wiener-Kronish, J. P. (2001) Type III protein secretion is associated with death in lower respiratory and systemic *Pseudomonas aeruginosa* infections. *J. Infect. Dis. 183*, 1767–1774.
10. Sawa, T., Yahr, T. L., Ohara, M., Kurahashi, K., Gropper, M. A., Wiener-Kronish, J. P., and Frank, D. W. (1999) Active and passive immunization with the *Pseudomonas* V antigen protects against type III intoxication and lung injury. *Nat. Med. 5*, 392–398.
11. Furukawa, S., Kuchma, S. L., and O'Toole, G. A. (2006) Keeping their options open: acute versus persistent infections. *J. Bacteriol. 188*, 1211–1217.
12. Goodman, A. L., Kulasekara, B., Rietsch, A., Boyd, D., Smith, R. S., and Lory, S. (2004) A signaling network reciprocally regulates genes associated with acute infection and chronic persistence in *Pseudomonas aeruginosa*. *Dev. Cell 7*, 745–754.
13. Yahr, T. L., and Greenberg, E. P. (2004) The genetic basis for the commitment to chronic versus acute infection in *Pseudomonas aeruginosa*. *Mol. Cell 16*, 497–498.
14. Engel, J., and Balachandran, P. (2009) Role of *Pseudomonas aeruginosa* type III effectors in disease. *Curr. Opin. Microbiol. 12*, 61–66.
15. Fraylick, J. E., La Rocque, J. R., Vincent, T. S., and Olson, J. C. (2001) Independent and coordinate effects of ADP-ribosyltransferase and GTPase-activating activities of exoenzyme S on HT-29 epithelial cell function. *Infect. Immun. 69*, 5318–5328.
16. Krall, R., Sun, J., Pederson, K. J., and Barbieri, J. T. (2002) In vivo rho GTPase-activating protein activity of *Pseudomonas aeruginosa* cytotoxin ExoS. *Infect. Immun. 70*, 360–367.
17. Sun, J., and Barbieri, J. T. (2003) *Pseudomonas aeruginosa* ExoT ADP-ribosylates CT10 regulator of kinase (Crk) proteins. *J. Biol. Chem. 278*, 32794–32800.
18. Finck-Barbanócon, V., Goranson, J., Zhu, L., Sawa, T., Wiener-Kronish, J. P., Fleiszig, S. M., Wu, C., Mende-Mueller, L., and Frank, D. W. (1997) ExoU expression by *Pseudomonas aeruginosa* correlates with acute cytotoxicity and epithelial injury. *Mol. Microbiol. 25*, 547–557.
19. Yahr, T. L., Hovey, A. K., Kulich, S. M., and Frank, D. W. (1995) Transcriptional analysis of the *Pseudomonas aeruginosa* exoenzyme S structural gene. *J. Bacteriol. 177*, 1169–1178.
20. Yahr, T. L., and Frank, D. W. (1994) Transcriptional organization of the trans-regulatory locus which controls exoenzyme S synthesis in *Pseudomonas aeruginosa*. *J. Bacteriol. 176*, 3832–3838.
21. Frank, D. W., Nair, G., and Schweizer, H. P. (1994) Construction and characterization of chromosomal insertional mutations of the *Pseudomonas aeruginosa* exoenzyme S trans-regulatory locus. *Infect. Immun. 62*, 554–563.
22. Frank, D. W. (1997) The exoenzyme S regulon of *Pseudomonas aeruginosa*. *Mol. Microbiol. 26*, 621–629.
23. Zheng, Z., Chen, G., Joshi, S., Brutinel, E. D., Yahr, T. L., and Chen, L. (2007) Biochemical characterization of a regulatory cascade controlling transcription of the *Pseudomonas aeruginosa* type III secretion system. *J. Biol. Chem. 282*, 6136–6142.
24. Parsot, C., Hamiaux, C., and Page, A. L. (2003) The various and varying roles of specific chaperones in type III secretion systems. *Curr. Opin. Microbiol. 6*, 7–14.
25. Feldman, M. F., and Cornelis, G. R. (2003) The multitalented type III chaperones: all you can do with 15 kDa. *FEMS Microbiol. Lett. 219*, 151–158.
26. Luo, Y., Bertero, M. G., Frey, E. A., Pfuetzner, R. A., Wenk, M. R., Creagh, L., Marcus, S. L., Lim, D., Sicheri, F., Kay, C., Haynes, C., Finlay, B. B., and Strynadka, N. C. (2001) Structural and biochemical characterization of the type III secretion chaperones CesT and SigE. *Nat. Struct. Biol. 8*, 1031–1036.
27. Rumpel, S., Lakshmi, R., Becker, S., and Zweckstetter, M. (2008) Assignment-free solution NMR method reveals CesT as an unswapped homodimer. *Protein Sci. 17*, 2015–2019.
28. van Eerde, A., Hamiaux, C., Perez, J., Parsot, C., and Dijkstra, B. W. (2004) Structure of Spa15, a type III secretion chaperone from *Shigella flexneri* with broad specificity. *EMBO Rep. 5*, 477–483.
29. Singer, A. U., Desveaux, D., Betts, L., Chang, J. H., Nimchuk, Z., Grant, S. R., Dangl, J. L., and Sondek, J. (2004) Crystal structures of the type III effector protein AvrPphF and its chaperone reveal residues required for plant pathogenesis. *Structure 12*, 1669–1681.
30. Birtalan, S., and Ghosh, P. (2001) Structure of the *Yersinia* type III secretory system chaperone SycE. *Nat. Struct. Biol. 8*, 974–978.
31. Locher, M., Lehnert, B., Krauss, K., Heesemann, J., Groll, M., and Wilharm, G. (2005) Crystal structure of the *Yersinia enterocolitica* type III secretion chaperone SycT. *J. Biol. Chem. 280*, 31149–31155.
32. Stebbins, C. E., and Galan, J. E. (2001) Maintenance of an unfolded polypeptide by a cognate chaperone in bacterial type III secretion. *Nature 414*, 77–81.
33. Lilic, M., Vujanac, M., and Stebbins, C. E. (2006) A common structural motif in the binding of virulence factors to bacterial secretion chaperones. *Mol. Cell 21*, 653–664.
34. Schubot, F. D., Jackson, M. W., Penrose, K. J., Cherry, S., Tropea, J. E., Plano, G. V., and Waugh, D. S. (2005) Three-dimensional structure of a macromolecular assembly that regulates type III secretion in *Yersinia pestis*. *J. Mol. Biol. 346*, 1147–1161.
35. Birtalan, S. C., Phillips, R. M., and Ghosh, P. (2002) Three-dimensional secretion signals in chaperone-effector complexes of bacterial pathogens. *Mol. Cell 9*, 971–980.

36. Phan, J., Tropea, J. E., and Waugh, D. S. (2004) Structure of the *Yersinia pestis* type III secretion chaperone SycH in complex with a stable fragment of YscM2. *Acta Crystallogr., Sect. D: Biol. Crystallogr. 60*, 1591–1599.
37. Thibault, J., Faudry, E., Ebel, C., Attree, I., and Elsen, S. (2009) Anti-activator ExsD forms a 1:1 complex with ExsA to inhibit transcription of type III secretion operons. *J. Biol. Chem. 284*, 15762–15770.
38. Bernhards, R. C., Jing, X., Vogelaar, N. J., Robinson, H., and Schubot, F. D. (2009) Structural evidence suggests that antiactivator ExsD from *Pseudomonas aeruginosa* is a DNA binding protein. *Protein Sci. 18*, 503–513.
39. McCaw, M. L., Lykken, G. L., Singh, P. K., and Yahr, T. L. (2002) ExsD is a negative regulator of the *Pseudomonas aeruginosa* type III secretion regulon. *Mol. Microbiol. 46*, 1123–1133.
40. Dasgupta, N., Lykken, G. L., Wolfgang, M. C., and Yahr, T. L. (2004) A novel anti-anti-activator mechanism regulates expression of the *Pseudomonas aeruginosa* type III secretion system. *Mol. Microbiol. 53*, 297–308.
41. Rietsch, A., Vallet-Gely, I., Dove, S. L., and Mekalanos, J. J. (2005) ExsE, a secreted regulator of type III secretion genes in *Pseudomonas aeruginosa*. *Proc. Natl. Acad. Sci. U.S.A. 102*, 8006–8011.
42. Urbanowski, M. L., Lykken, G. L., and Yahr, T. L. (2005) A secreted regulatory protein couples transcription to the secretory activity of the *Pseudomonas aeruginosa* type III secretion system. *Proc. Natl. Acad. Sci. U.S.A. 102*, 9930–9935.
43. Lykken, G. L., Chen, G., Brutinel, E. D., Chen, L., and Yahr, T. L. (2006) Characterization of ExsC and ExsD self-association and heterocomplex formation. *J. Bacteriol. 188*, 6832–6840.
44. Nallamsetty, S., Austin, B. P., Penrose, K. J., and Waugh, D. S. (2005) Gateway vectors for the production of combinatorially-tagged His6-MBP fusion proteins in the cytoplasm and periplasm of *Escherichia coli*. *Protein Sci. 14*, 2964–2971.
45. Tropea, J. E., Phan, J., and Waugh, D. S. (2006) Overproduction, purification, and biochemical characterization of the dual specificity H1 protein phosphatase encoded by variola major virus. *Protein Expression Purif. 50*, 31–36.
46. Doublie, S. (2007) Production of selenomethionyl proteins in prokaryotic and eukaryotic expression systems. *Methods Mol. Biol. 363*, 91–108.
47. Gattiker, A., Bienvenut, W. V., Bairoch, A., and Gasteiger, E. (2002) FindPept, a tool to identify unmatched masses in peptide mass fingerprinting protein identification. *Proteomics 2*, 1435–1444.
48. Otwinowski, Z. M. W. (1997) HKL2000. *Methods Enzymol. 276*, 307–326.
49. Zwart, P. H., Afonine, P. V., Grosse-Kunstleve, R. W., Hung, L. W., Ioerger, T. R., McCoy, A. J., McKee, E., Moriarty, N. W., Read, R. J., Sacchettini, J. C., Sauter, N. K., Storoni, L. C., Terwilliger, T. C., and Adams, P. D. (2008) Automated structure solution with the PHENIX suite. *Methods Mol. Biol. 426*, 419–435.
50. Emsley, P., and Cowtan, K. (2004) Coot: model-building tools for molecular graphics. *Acta Crystallogr., Sect. D: Biol. Crystallogr. 60*, 2126–2132.
51. Laskowski, R. A., MacArthur, M. W., Moss, D. S., and Thornton, J. M. (1993) PROCHECK: a program to check the steriochemical quality of protein structures. *J. Appl. Crystallogr. 26*, 282–291.
52. Sussman, J. L., Lin, D., Jiang, J., Manning, N. O., Prilusky, J., Ritter, O., and Abola, E. E. (1998) Protein Data Bank (PDB): database of three-dimensional structural information of biological macromolecules. *Acta Crystallogr., Sect. D: Biol. Crystallogr. 54*, 1078–1084.
53. Landau, M., Mayrose, I., Rosenberg, Y., Glaser, F., Martz, E., Pupko, T., and Ben-Tal, N. (2005) ConSurf 2005: the projection of evolutionary conservation scores of residues on protein structures. *Nucleic Acids Res. 33*, W299–302.
54. Holm, L., Kaariainen, S., Rosenstrom, P., and Schenkel, A. (2008) Searching protein structure databases with DaliLite v.3. *Bioinformatics 24*, 2780–2781.
55. Rodgers, L., Gamez, A., Riek, R., and Ghosh, P. (2008) The type III secretion chaperone SycE promotes a localized disorder-to-order transition in the natively unfolded effector YopE. *J. Biol. Chem. 283*, 20857–20863.
56. Parsot, C., Hamiaux, C., and Page, A. L. (2003) The various and varying roles of specific chaperones in type III secretion systems. *Curr. Opin. Microbiol. 6*, 7–14.
57. (1994) The CCP4 suite: programs for protein crystallography, Acta Crystallogr., Sect. D: Biol. Crystallogr. *50*, 760−763.
58. Blundell, T. L., and Johnson, L. N. (1976) Protein Crystallography, Academic Press, London.
59. Brunger, A. T. (1992) Free R value: a novel statistical quantity for assessing the accuracy of crystal structures. *Nature 355*, 472–475.
60. DeLano, W. L. (2001) The PyMOL Molecular Graphics System, DeLano Scientific LLC, San Carlos, CA (http://www.pymol.org).
61. Gouet, P., Robert, X., and Courcelle, E. (2003) ESPript/ENDscript: extracting and rendering sequence and 3D information from atomic structures of proteins. *Nucleic Acids Res. 31*, 3320–3323.
62. Wallace, A. C., Laskowski, R. A., and Thornton, J. M. (1995) LIGPLOT: a program to generate schematic diagrams of protein-ligand interactions. *Protein Eng. 8*, 127–134.